Generalized Turing Patterns and Their Selective Realization in Spatiotemporal Systems

Govindan Rangarajan[1], Yonghong Chen[2] and Mingzhou Ding[2]
[1]*Department of Mathematics and Center for Theoretical Studies, Indian Institute of Science, Bangalore 560 012, India*
[2]*Center for Complex Systems and Brain Sciences, Florida Atlantic University, Boca Raton, FL 33431, USA*

Abstract

We consider the pattern formation problem in coupled identical systems after the global synchronized state becomes unstable. Based on analytical results relating the coupling strengths and the instability of each spatial mode (pattern) we show that these spatial patterns can be selectively realized by varying the coupling strengths along different paths in the parameter space. Furthermore, we discuss the important role of the synchronized state (fixed point versus chaotic attractor) in modulating the temporal dynamics of the spatial patterns.

Introduction. In a reaction-diffusion system, at the Turing bifurcation point the global equilibrium state becomes unstable and an inhomogeneous spatial pattern known as a Turing pattern [1] emerges. Following Turing's classic work pattern formation in reaction-diffusion systems has become a major topic of investigation both theoretically and experimentally [2,3].

The idea in Turing's original formulation is not limited to just reaction-diffusion systems with a single diffusion constant. Networks where the diffusion is characterized by a more complex function and networks where the coupling is not diffusive can be studied in a similar fashion. This makes the idea of pattern formation applicable to diverse areas of science and engineering [4–11]. Furthermore, the globally synchronized state prior to the formation of spatial patterns need not be a fixed point as in Turing's original case. One can consider synchronized limit cycles and chaotic attractors as the bifurcating state. When the synchronized state becomes unstable under parameter variation, the dynamics may exit the synchronization manifold along certain eigen-mode, giving rise to a spatial pattern. We refer to these patterns as Generalized Turing Patterns (GTPs).

GTPs have been the subject of several recent publications [10]. These papers mainly rely on numerical techniques to obtain the threshold of instabilities. In this letter we focus on the analytical treatment of the pattern formation and pattern selection. To do so we restrict ourselves to networks in which each node is coupled to its P nearest neighbors. Under the assumption of periodic boundary condition and translational invariance the eigen-modes are the spatial Fourier modes. Our main results are as follows. First, we derive explicit analytical expressions defining the stability region in the parameter space spanned by the coupling strengths. Second, we demonstrate that, by following different paths in the parameter space, different spatiotemporal patterns can be selectively realized. Third, although the spatial patterns are the same for a given coupling matrix, we show that, depending on whether we have a synchronized fixed point or chaotic attractor, the temporal evolution of the patterns is either constant in time or modulated in an on-off intermittent fashion. We study networks on both one dimensional (1-d) and two dimensional (2-d) lattices. Only coupled maps are considered here. Similar results apply to coupled differential equations.

One dimensional lattices. Consider the following 1-d coupled map lattice where each node is coupled to its P nearest neighbors in a general diffusive manner:

$$\mathbf{x}_j(n+1) = \mathbf{f}(\mathbf{x}_j(n)) + \frac{1}{2P}\sum_{p=1}^{P} a_p \left[\mathbf{f}(\mathbf{x}_{j+p}(n)) + \mathbf{f}(\mathbf{x}_{j-p}(n)) - 2\mathbf{f}(\mathbf{x}_j(n))\right], \quad j = 1, 2, \ldots, L. \tag{1}$$

Here the M-dimensional vector $\mathbf{x}_j$ describes the map at the jth node of the lattice, a_p's denote the coupling strengths and n is the time index. We impose the periodic boundary condition: $\mathbf{x}_{j+L}(n) = \mathbf{x}_j(n)$. Since the coupling strengths don't depend on the spatial position index j we have translational invariance. The individual (uncoupled) map is $\mathbf{x}_j(n+1) = \mathbf{f}(\mathbf{x}_j(n))$.

Clearly the synchronized state $\mathbf{x}_j = \mathbf{x}$, $\forall\ j$ is a solution of the above system. To study its stability we linearize Eq. (1) around the synchronized state $\mathbf{x}$ to obtain:

$$\mathbf{z}_j(n+1) = \mathbf{J}(\mathbf{x}(n))\mathbf{z}_j(n) + \mathbf{J}(\mathbf{x}(n))\frac{1}{2P}\sum_{p=1}^{P} a_p[\mathbf{z}_{j+p}(n) + \mathbf{z}_{j-p}(n) - 2\mathbf{z}_j(n)], \tag{2}$$

where $\mathbf{z}_j$ denotes the jth map's deviations from $\mathbf{x}$ and $\mathbf{J}$ is the $M \times M$ Jacobian matrix corresponding to $\mathbf{f}$. Consider the discrete Fourier transform of $\mathbf{z}_j$:

$$\boldsymbol{\eta}_l(n) = \frac{1}{L}\sum_{j=1}^{L} \exp(-i2\pi jl/L)\mathbf{z}_j(n). \tag{3}$$

Performing the discrete Fourier transform on the linearized equation we get

$$\boldsymbol{\eta}_l(n+1) = \mathbf{J}(\mathbf{x}(n)) \left[\boldsymbol{\eta}_l(n) + \frac{1}{2P}\sum_{p=1}^{P} a_p \left(\exp(i2\pi pl/L) + \exp(-i2\pi pl/L) - 2\right)\boldsymbol{\eta}_l(n)\right]. \tag{4}$$

Simplifying we finally have

$$\boldsymbol{\eta}_l(n+1) = \mathbf{J}(\mathbf{x}(n)) \left[1 - \frac{2}{P}\sum_{p=1}^{P} a_p \sin^2(\pi pl/L)\right]\boldsymbol{\eta}_l(n). \tag{5}$$

We start by examining the case where the individual maps are chaotic and $\mathbf{x}$ corresponds to the synchronized chaotic state. The synchronized state is stable if all the transverse Lyapunov exponents are negative [11,12]. Computing the Lyapunov exponents μ_i of the above linearized equation we get

$$\mu_i(l) = h_i + \ln|1 - \frac{2}{P}\sum_{p=1}^{P} a_p \sin^2(\pi pl/L)|, \quad i = 1, 2, \ldots, M, \tag{6}$$

where h_i's are the Lyapunov exponents for the individual map ordered as $h_1 \geq h_2 \geq \cdots \geq h_M$. Note that the $l = 0$ Fourier mode corresponds to the synchronized chaotic state where the Lyapunov exponents of the coupled system are given by the Lyapunov exponents of the individual system. For each $l \neq 0$ value, $\mu_1(l)$ gives the largest transverse Lyapunov exponent. Therefore, stability of the synchronized chaotic state is ensured if $\mu_1(l) < 0$ for all $l \neq 0$. By symmetry of the Fourier modes, we only need to consider $\mu_1(l) < 0$ for $l = 1, 2, \ldots L/2$ (if L is odd, we take $(L-1)/2$). Thus we have the stability conditions

$$|1 - \frac{2}{P}\sum_{p=1}^{P} a_p \sin^2(\pi pl/L)| < \exp(-h_1), \quad l = 1, 2, \ldots L/2 \text{ or } (L-1)/2. \tag{7}$$

This set of inequalities defines a stability region in the parameter space spanned by the a_p's. By selecting a given Fourier mode and choosing a suitable path in the parameter space we can realize the corresponding GTP. Note that, if one considers only the nearest neighbor diffusive coupling ($P = 1$), the parameter space is one dimensional and at most two GTPs can be excited by varying the coupling strength even though there are many possible modes. By enlarging the parameter space we obtain much greater variety in terms of GTPs that can be realized. With recent progress [13] in obtaining stability conditions for general coupling matrices, we are currently investigating whether even more general Turing patterns can be obtained.

As a numerical example we consider coupled logistic maps in the chaotic regime where $f(x) = 1 - ax^2$ with $a = 1.9$. The maximum Lyapunov exponent h_1 is 0.549. For simplicity,

we restrict ourselves to $L = 5$ and $P = 2$. The stability conditions for the synchronized chaotic state are:

$$-0.578 < 1 - a_1 \sin^2(\pi l/5) - a_2 \sin^2(2\pi l/5) < 0.578, \quad l = 1, 2 \tag{8}$$

which give the stability region marked black in the parameter plane [Fig. 1(a)]. We call the $l = 1$ mode the long wavelength (LW) pattern and the $l = 2$ mode the short wavelength (SW) pattern. The arrows indicate the paths along which either of the two patterns can be selected.

The main frame in Fig. 1(b) shows the temporal dynamics of the long wavelength pattern for $a_1 = 0.96$ and $a_2 = 0.1$. Here deviations from the synchronization manifold is approximated by

$$z_j(n) = x_j(n) - \sum_{j=1}^{L} x_j(n)/L$$

with $L = 5$. To facilitate visualization, at each time step n, a continuous function is splined through the six discrete nodes: $z_1(n)$, $z_2(n)$, $\cdots$, $z_5(n)$, and $z_6(n) = z_1(n)$. Furthermore, to overcome the distortion due to the two opposite phases of a pattern, we monitor the deviation at a given node and multiple the deviations at every node by a minus sign whenever the deviation at the monitored node becomes negative.

Since the bifurcation undergone by the system at the boundary of the stability region is the blow-out bifurcation and there is only one attractor prior to the bifurcation, the dynamics in this case is referred to as on-off intermittency [12,14]. The temporal evolution of the deviations at a typical node is given by the curve to the left of the main pattern frame. Its bursting behavior is characteristic of on-off intermittency. The GTP itself is given at the bottom of Fig. 1(b).

For $a_1 = 0.04$ and $a_2 = 1.1$ we observe the short wavelength pattern in Fig. 1(c). The same visualization methods are used to make this figure.

To understand how the synchronized state shapes the temporal properties of the GTP after desynchronization we consider a case where the synchronized state is a fixed point. Again we use the coupled logistic maps and choose $a = 0.5$. The fixed point is $\bar{x} = 0.73$ and the lyapunov exponent is $h_1 = -0.31$. Still letting $L = 5, P = 2$, we get the stability region defined by

$$-1.36 < 1 - a_1 \sin^2(\pi l/5) - a_2 \sin^2(2\pi l/5) < 1.36, \quad l = 1, 2 \tag{9}$$

shown in Fig. 2(a). Following the arrows we can realize either the long or the short wavelength patterns. Figure 2(b) gives the long wavelength pattern for $a_1 = 0.5$ and $a_2 = 2.5$ and Fig. 2(c) gives the short wavelength pattern for $a_1 = 2.5$ and $a_2 = 0.5$. The same methods of plotting as that used for Figure 1 are used here. Comparing Figs. 2(b) and (c) with Figs. 1(b) and (c) we see the same spatial patterns but different temporal behaviors.

For the example in Fig. 2 the final GTPs are the new fixed points displayed as a function of the space coordinate. Predicting the exact location of these new fixed points requires the nonlinear terms dropped in the linear stability analysis. Although it is often the case that the spatial functions underlying the new fixed points agree with the respective linear eigenmodes this is by no means a guaranteed fact [2]. On the other hand, when the synchronized

state is chaotic, linear analysis will govern the temporal evolution whenever the phase space trajectory comes back to near the synchronization manifold.

Two dimensional lattices. Finally, we consider a 2-d coupled map lattice given by

$$\mathbf{x}_{j,k}(n+1) = \mathbf{f}(\mathbf{x}_{j,k}(n)) + \frac{1}{2P}\sum_{p=1}^{P}\{a_p\left[\mathbf{f}(\mathbf{x}_{j+p,k}(n)) + \mathbf{f}(\mathbf{x}_{j-p,k}(n))\right] \\ +b_p\left[\mathbf{f}(\mathbf{x}_{j,k+p}(n)) + \mathbf{f}(\mathbf{x}_{j,k-p}(n))\right] - 2(a_p+b_p)\mathbf{f}(\mathbf{x}_{j,k}(n))\}, \quad j,k = 1,2,\ldots,L. \tag{10}$$

Linearizing around the synchronized state $\mathbf{x}_{j,k} = \mathbf{x},\ \forall\ j,k$, we get

$$\mathbf{z}_{j,k}(n+1) = \mathbf{J}(\mathbf{x}(n))\mathbf{z}_{j,k}(n) + \mathbf{J}(\mathbf{x}(n))\frac{1}{2P}\sum_{p=1}^{P}\{a_p[\mathbf{z}_{j+p,k}(n) + \mathbf{z}_{j-p,k}(n)]+ \\ b_p[\mathbf{z}_{j,k+p}(n) + \mathbf{z}_{j,k-p}(n)] - 2(a_p+b_p)\mathbf{z}_{j,k}(n)\}, \tag{11}$$

where $\mathbf{z}$ denotes the deviation from the synchronized manifold. Applying the 2-d discrete Fourier transformation given by

$$\boldsymbol{\eta}_{l,m}(n) = \frac{1}{L^2}\sum_{j=1}^{L}\sum_{k=1}^{L}\exp(-i2\pi jl/L)\exp(-i2\pi km/L)\mathbf{z}_{j,k}(n), \tag{12}$$

to the linearized equation and simplifying we finally obtain

$$\boldsymbol{\eta}_{l,m}(n+1) = \mathbf{J}(\mathbf{x}(n))\left[1 - \frac{2}{P}\sum_{p=1}^{P}\left(a_p\sin^2(\pi pl/L) + b_p\sin^2(\pi pm/L)\right)\right]\boldsymbol{\eta}_{l,m}(n). \tag{13}$$

Proceeding as before, the stability conditions for synchronized state are given by

$$|1 - \frac{2}{P}\sum_{p=1}^{P}\left(a_p\sin^2(\pi pl/L) + b_p\sin^2(\pi pm/L)\right)| < \exp(-h_1), \\ l,m = 0,1,2,\ldots L/2 \text{ or } (L-1)/2, \tag{14}$$

with $l = m = 0$ excluded (as it corresponds to the synchronized manifold).

As in the 1-d lattice case, GTPs emerge when the synchronized state loses its stability. This happens when the parameters are varied across the stability boundary. We can select a particular (l,m) mode and have it realized by appropriately choosing the coupling strengths a_p and b_p $(p = 1,2,\ldots,P)$. We will again illustrate this with logistic maps coupled together on a 2-d lattice. We set $a = 1.5$. Then $h_1 = 0.231$. Choose $L = 5$ and $P = 1$ for simplicity. The stability conditions are

$$-0.79 < 1 - \frac{a_1}{2}\sin^2(\pi l/5) - \frac{b_1}{2}\sin^2(\pi m/5) < 0.79, \quad l,m = 0,1,2, \tag{15}$$

with $l = m = 0$ excluded. Figure 3(a) depicts the stability region (black). Different edges of the region are the instability thresholds of different modes. It is obvious that only the (0,1), (1,0) and (2,2) modes can be observed given two tuning parameters. By including additional coupling strengths not considered here one can potentially make the (1,1), (1,2) and (2,1) modes observable. Figure 3(b) shows a snapshot of deviations from the synchronization

manifold at different nodes for $a_1 = 0.5$ and $b_1 = 0.5$. As before a continuous function is fitted through all the nodes. Although not perfect the essential features of a (2,2) pattern is quite clearly visible in the snapshot. The other two patterns (0,1) and (1,0) can be similarly realized by choosing proper parameters with respect to the boundary of the stability region in Fig. 3(a).

We thank Jianfeng Feng for helpful comments. The work was supported by US ONR Grant N00014-99-1-0062. GR was also supported by the Homi Bhabha Fellowship and by DRDO and ISRO, India.

REFERENCES

[1] A. M. Turing, Phil. Trans. Roy. Soc. B **237**, 37 (1952).

[2] J. D. Murray, Mathematical Biology (Springer, Berlin, 1993).

[3] Q. Ouyang and H. L. Swinney, Nature **352** 610 (1991); H. Meinhardt, Rep. Prog. Phys. **55**, 797 (1992); P. Hohenberg and M. Cross, Rev. Mod. Phys. **65** 3 (1993); J. E. Pearson, Science **261**, 189 (1993); K. J. Lee et. al., Nature **369**, 215 (1994); S. Kondo and R. Asai, Nature **376**, 765 (1995); M. Seul and D. Andelman, Science **267**, 476 (1995); V. Petrov et. al., Phys. Rev. Lett. **75**, 2895 (1995); V. Petrov, Q. Ouyang and H. L. Swinney, Nature **388**, 655 (1997); Y. Jiang et. al., Phys. Rev. E **56**, 2568 (1997); S. Sinha and N. Gupte, Phys. Rev. E **58**, R5221 (1998); C. A. Klausmeier, Science **284**, 1826 (1999); R. A. Satnoianu, M. Menzinger and P. K. Maini, J. Math. Biol. **41**, 493 (2000); Y. J. Li et. al., Science **291**, 2395 (2001); M. R. Roussel and J. Wang, Phys. Rev. Lett. **87**, 188302 (2001); L. Yang et. al., Phys. Rev. Lett. **88**, 208303 (2002); M. G. Neubert, H. Caswell and J. D. Murray, Math. Biosci. **175**, 1 (2002).

[4] K. Kaneko, Prog. Theor. Phys. **72**, 480 (1984); L. M. Pecora and T. L. Carroll, Phys. Rev. Lett. **64**, 821 (1990); R. E. Amritkar, P. M. Gade, A. D. Gangal, V. M. Nandakumaran, Phys. Rev. A **44**, R3407 (1991); Q. Zhilin and H. Gang, Phys. Rev. E **49**, 1099 (1994); J. F. Heagy, L. M. Pecora and T. L. Carroll, Phys. Rev. E **50**, 1874 (1994); N. Chatterjee and N. Gupte, Phys. Rev. E **53**, 4457 (1996); D. J. Gauthier and J. C. Bienfang, Phys. Rev. Lett. **77**, 1751 (1996); Y.C. Lai, Y. Naigai and C. Grebogi, Phys. Rev. Lett. **79**, 652(1997); P. M. Gade and C.K. Hu, Phys. Rev. E **62** 6409 (2000); K. Zhu and T. Chen, Phys. Rev. E **63**, 067201 (2001); J. Jost and M. P. Joy, Phys. Rev. E **65**, 016201 (2002), M. Barahona and L. M. Pecora, Phys. Rev. Lett. **89**, 054101 (2002).

[5] L. Kocarev and U. Parlitz, Phys. Rev. Lett. **76**, 1816 (1996); R. Brown and N. F. Rulkov, Phys. Rev. Lett. **78**, 4189 (1997); P. Glendinning, Phys. Lett. A **259**, 129 (1999); V. N. Belykh, I. V. Belykh and M. Hasler, Phys. Rev. E **62**, 6332 (2000); V. N. Belykh, I. V. Belykh and E. Mosekilde, Phys. Rev. E **63**, 036216 (2001).

[6] D. Hansel and H. Sompolinsky, Phys. Rev. Lett. **68**, 718 (1992); D. Hansel, Int. J. Neural Sys. **7**, 403 (1996); F. Pasemann, Physica D **128**, 236 (1999).

[7] H. G. Winful and L. Rahman, Phys. Rev. Lett. **65**, 1575 (1990); R. Li and T. Erneux, Opt. Commun. **99**, 196 (1993); R. Roy and K. S. Thornburg, Jr., Phys. Rev. Lett. 72, 2009 (1994); K. Otsuka et. al., Phys. Rev. Lett. **84**, 3049 (2000).

[8] C. W. Wu and L. O. Chua, IEEE Trans. on Circuits and Systems I **42**, 430 (1995); G. Filatrella, B. Straughn and P. Barbara, J. of Appl. Phys. **90**, 5675 (2001); J. Ito and K. Kaneko, Phys. Rev. Lett. **88**, 028701 (2002).

[9] K. M. Cuomo and A. V. Oppenheim, Phys. Rev. Lett. **71**, 65 (1993); L. M. Pecora et. al., Chaos **7**, 520 (1997) and references therein.

[10] J.F. Heagy, L.M. Pecora and T.L. Carroll, Phys. Rev. Lett. **74**, 4185(1995); L.M. Pecora, Phys. Rev. E **58**, 347(1998); S. Wang et. al., preprint.

[11] G. Rangarajan and M. Ding, Phys. Lett. A **296**, 204 (2002).

[12] We note that, since the Lyapunov exponents are computed from typical initial conditions, the stability discussed for synchronized chaos here and below is with respect to the blow-out bifurcation. Bubbling transition can occur while the parameters are still within the bound derived in this work. For details on these phenomena see E. Ott and J.C. Sommerer, Phys. Lett. A **188**, 39(1994); P. Ashwin, J. Buescu and I. Stewart,

Phys. Lett. **193**, 126(1994); S.C. Venkataramani et al, Phys. Rev. Lett. **77**, 5361(1996); and S.C. Venkataramani et al, Phys. Rev. E **54**, 1346(1996).

[13] Y. Chen, G. Rangarajan and M. Ding (submitted) (2002).

[14] A. S. Pikovsky, Z. Phys. B **55**, 149 (1984); H. Fujisaka and T. Yamada, Prog. Theor. Phys. **74**, 918 (1985); N. Platt, E. A. Spiegel, and C. Tresser, Phys. Rev. Lett. **70**, 279 (1993); M. Ding and W. Yang, Phys. Rev. E *54*, 2489(1996); M. Ding and W. Yang, Phys. Rev. E **54**, 2489 (1996); M. Ding and W. Yang, Phys. Rev. E **56**, 4009 (1997).

FIGURE CAPTIONS

Figure 1: Pattern selection from the synchronized chaotic state in a 1-d map lattice ($P = 2$). In (a), the region of stable synchronization (black area) and distinct pattern selection directions are shown. In (b), temporal evolution of the long wavelength pattern is given with $a_1 = 0.96, a_2 = 0.1$. In (c), temporal evolution of the short wavelength pattern with $a_1 = 0.04, a_2 = 1.1$ is given.

Figure 2: Pattern selection from the synchronized equilibrium state in a 1-d map lattice ($P = 2$). In (a), the region of stable synchronization (black area) and distinct pattern selection directions are shown. In (b), the long wavelength pattern evolving as a fixed point in time is given with $a_1 = 0.5, a_2 = 2.2$. In (c), the short wavelength pattern with $a_1 = 2.2, a_2 = 0.5$ is shown.

Figure 3: Pattern selection in a 2-d map lattice ($P = 1$). In (a), the region of stable synchronization (black area) and the directions of selecting some patterns in the parameter space are given. In (b), a (2,2) pattern is shown with $a_1 = 0.5, b_1 = 0.5$.

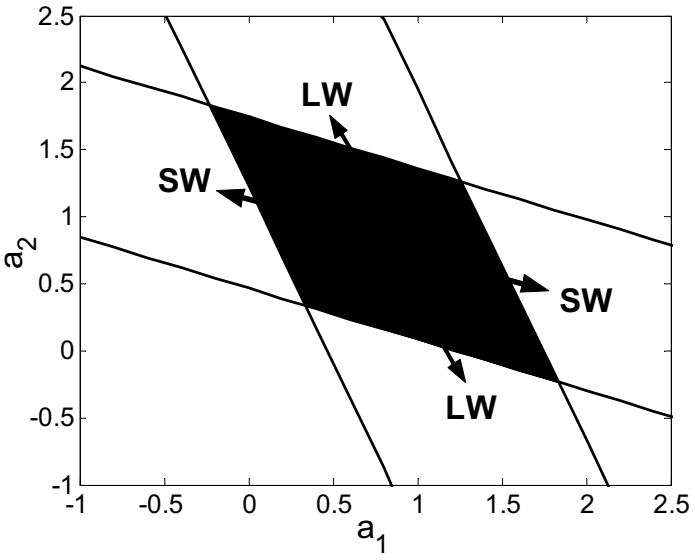
LW
SW
SW
LW
a2
a1
2.5
2
1.5
1
0.5
0
-0.5
-1
-1
-0.5
0
0.5
1
1.5
2
2.5

(a)

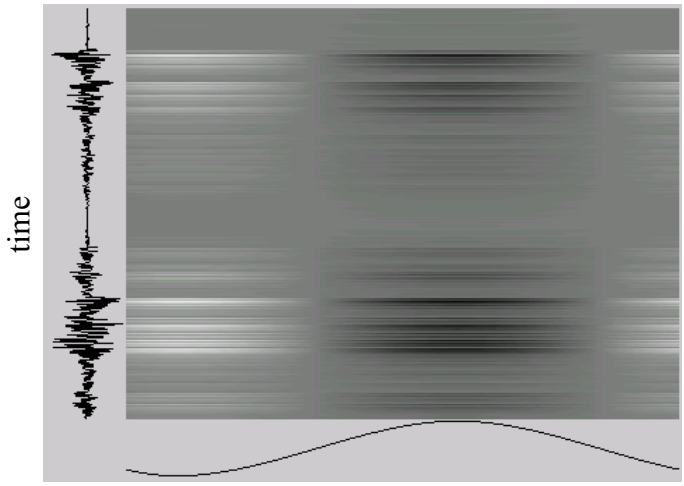
time
space

(b)

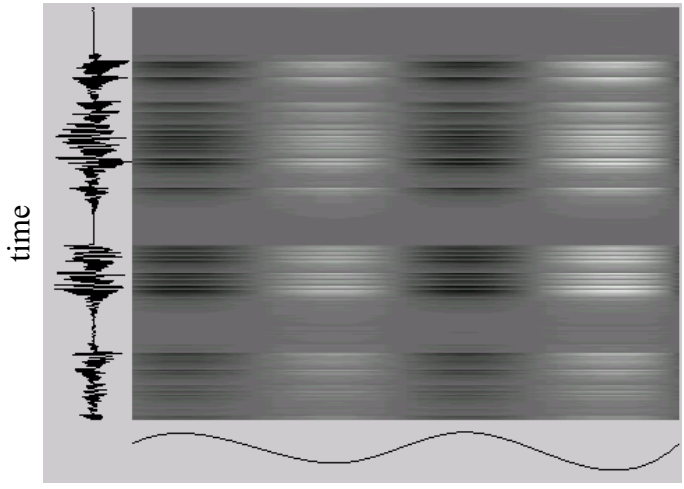
time
space

(c)

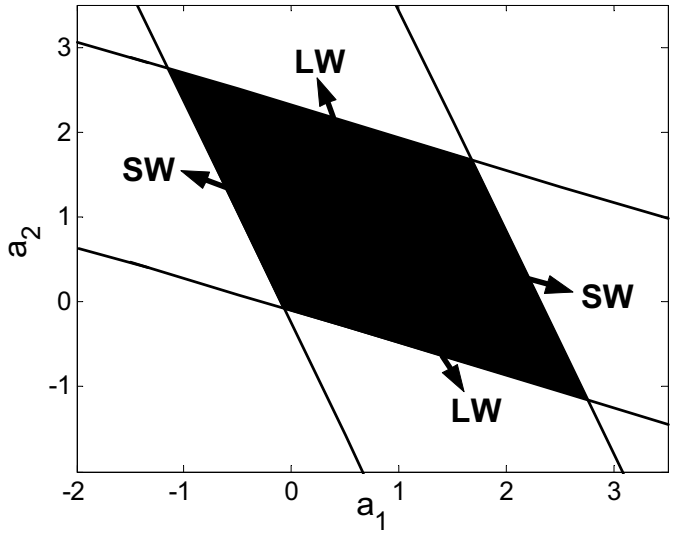

(a)

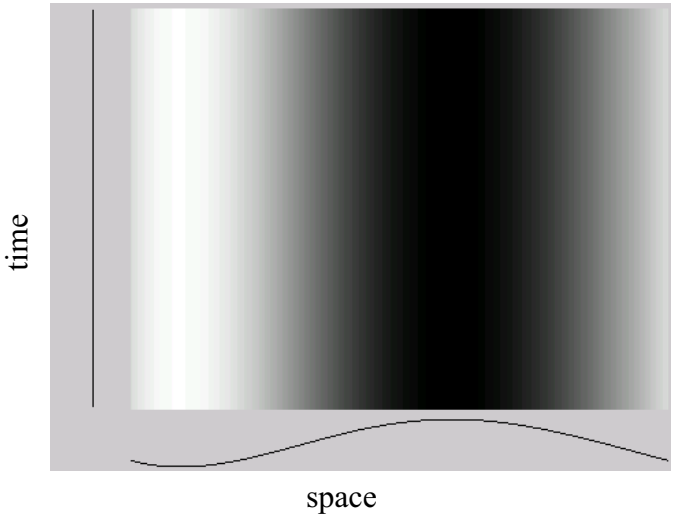

(b)

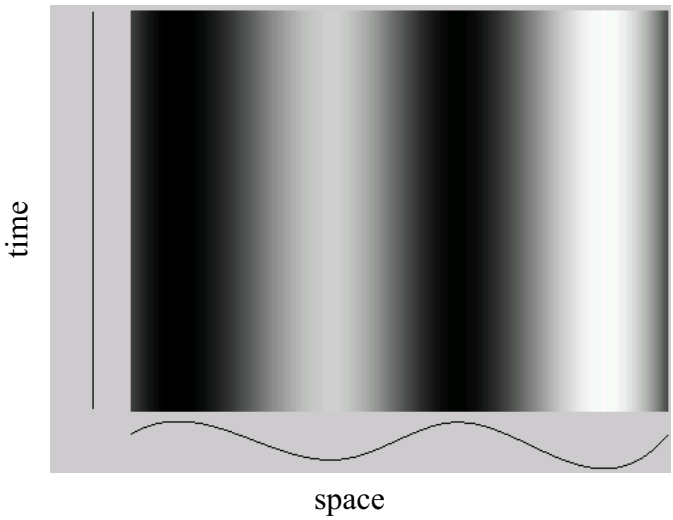

(c)

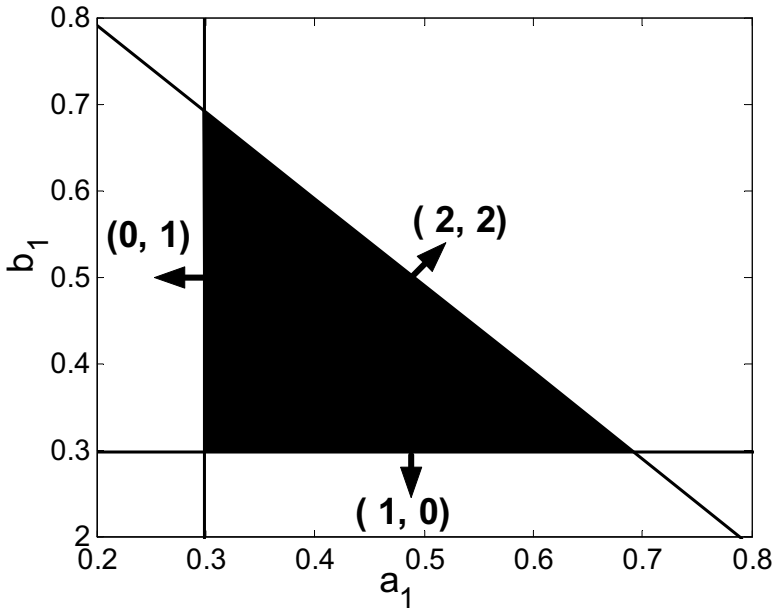

(a)

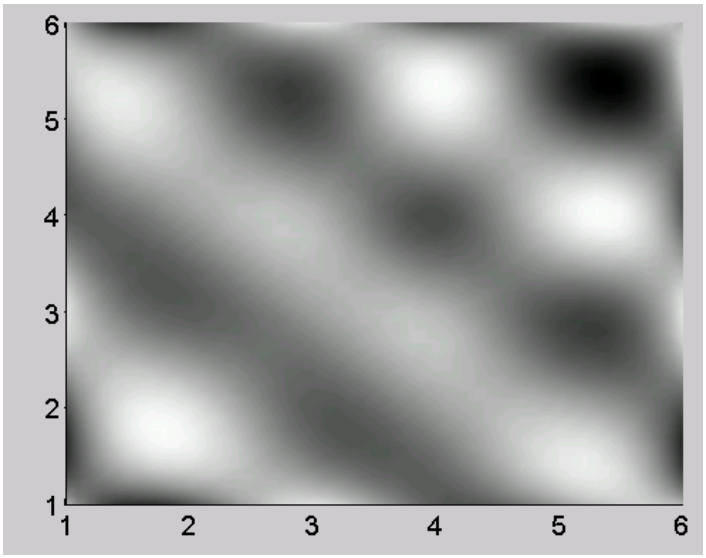

(b)